Characterization and antibacterial studies of Sn doped CuO nanocomposite using *centratherum punctatum* leaf extract

S. Subha[a,*], M. Nagarajan[a], S. Saseetha[a], S. C. Vella Durai[b]
[a]*Research Department of Physics, V. O. Chidambaram College, Thoothukudi-628008, Tamilnadu, India, Affiliated to Manonamaniam Sundaranar University, Abishekapatti, Tirunelveli, Tamil Nadu, India.*
[b]*PG and Research Department of Physics, Sri Paramakalyani College, Alwarkurichi – 627412, Tenkasi, Tamilnadu, India*

In order to synthesize CuO, SnO_2, and Sn doped CuO nanocomposites, accessible and non-toxic materials, specifically leaf extract from *Centratherum punctatum*, were used in this work to apply the concepts and practices of green chemistry. These methods are both economical and environmentally friendly. A comprehensive range of characterisation techniques, including as FTIR, X-ray diffraction, and UV-vis spectroscopy, were also used to confirm the structures of all the produced nanomaterials. Instead, FESEM and EDAX were used to analyze the morphologies and elemental composition of recently produced nanomaterials. A decline in the optical band gap values was indicated by the red shift observed in the UV-vis study following tin doping. A sample's presence of different functional groups is confirmed by FT-IR analysis. For CuO NPs, SnO_2, and Sn doped CuO NCs, the XRD results yielded crystallite sizes of 6 nm, 21 nm, and 29 nm, respectively, for the produced particles. The ferromagnetic, diamagnetic, and super paramagnetic characteristics of the produced samples at room temperature were validated by vibrating sample magnetometer experiments. Cyclic voltammetry is used to examine the nanoparticles' electrochemical analysis. Using Sn doped CuO nanocomposite material, it shows a high specific capacitance value of about ~187 Fg^{-1} at a current density of 10 mV/s. It was found from the electrochemical studies that the produced nanomaterials are suitable for capacitive behaviour. After all, the presence of inhibition zones surrounding each well led us to the conclusion that the nanoparticles exhibited antibacterial activity against the *pathogenic strains* of *Staphylococcus aureus* and *Escherichia coli*.

(Received January 21, 2024; Accepted April 15, 2024)

Keywords: Antibacterial, Biosynthesis, Centratherum punctatum leaves, Cyclic voltammetry

1. Introduction

The majority of research is concerned with the synthesis, characterization, and production of nanomaterials [1]. This is a consequence of the finding that, on occasion, some physical and chemical properties of nanomaterials might diverge dramatically from those of the bulk state [2]. The increasing applications of metal oxide nanoparticles in photocatalysis, biotechnology, optics, and medicine have made their manufacture simple and environmentally benign [3]. CuO's low bandgap of 1.2–2 eV, which qualifies it as a semiconductor, together with its antibacterial, mechanical, electrical, magnetic, and therapeutic properties, have attracted more attention than the others [4, 5]. Adding dopants to the parent system is one of the most important techniques to modify the attributes of a material. These dopants promoted the decrease in size, lowered the surface, and altered the shapes [6]. TMO nanoparticles can be produced using a variety of methods, including hydrothermal, sol-gel, sputtering, and co-precipitation. The use of dangerous chemicals in chemical synthesis procedures makes them non-ecofriendly [7]. In the field of TMO

* Corresponding author: ssadhithya@gmail.com
https://doi.org/10.15251/DJNB.2024.192.619

manufacturing, green synthesis shows promise and is favored since it is environmentally beneficial. Plant extracts from stems, leaves, flowers, peels, bacteria, fungus, and other parts of the plant work as reducing and capping agents in this process.

Among the many benefits of green synthesis are the inexpensive cost of plant extracts, short processing times, one-step reaction procedures, and highly effective biological products [8, 9, 10].

Therefore, the goal of this work is to create CuO, SnO_2, and Sn doped CuO nanocomposites and explores their diverse properties using Centratherum punctutam leaf extract. Leaf extract allows nanoparticles to change size and form in addition to preventing them from clumping. Renowned as the "Queen of All Herbs," *Centratherum punctatum* is closely related to the exceedingly valued medicinal plant Centratherum anthel methicum. In traditional medicine, *Centratherum punctatum*, a member of the Asteraceae family, is utilized. This perennial shrub is between forty and sixty centimeters tall. Purple flower heads adorn its well-branched stem [11, 12].

2. Materials and methods

2.1. Chemicals and reagents

Copper Chloride, Tin Chloride and Centratherum punctutam leaves were used. All the chemicals were purchased from Merck, Mumbai.

2.2. Extract preparation

Centratherum punctutam fresh leaves were gathered and properly cleaned with tap water first, then distilled water. Following the drying process, these leaves were diced into little bits. After being well cleaned, 10 g of Centratherum punctutam was soaked in 100 ml of deionized water and heated to 80 °C for an hour. To obtain a pure aqueous extract, the plant extract was chilled and filtered through Whatmann filter paper. At normal temperature, the aqueous extract's pH was found to be 5.5. The extract should only be kept for three days in the refrigerator.

2.3. Green synthesis of CuO, SnO_2 nanoparticles

To prepare CuO nanoparticles (0.1 M), 100 ml of Copper Chloride ($CuCl_2.2H_2O$) solution was prepared, mixed with 40 ml of leaf extract, and the resultant mixture was stirred for one hour. Finally, the blue colour of copper chloride changed from bluish-green to dark green and a brown colour precipitate was formed. The precipitate formed was rinsed several times with deionised water to remove the impurities and then filtered using No:1 Whatman filter paper dried at 100^0 C at room temperature. The resulting powder was calcined for one hour at 500 ^{0}C. Finally, the black-coloured CuO nanoparticles were collected and stored for further characterization. SnO_2 was prepared separately by taking tin chloride as precursor through the similar procedure

2.4 Green Synthesis of Sn doped CuO nanocomposite

The Sn doped CuO nanocomposite were synthesized according to Soruma Gudina Firisa [13] with some modifications. In this procedure, 50 ml of 0.1 M copper chloride and 10 ml of 0.1 M tin chloride were separately prepared. 20 ml of leaf extract was added to the copper chloride solution and stirred for 30 minutes to prepare the CuO nanoparticles. Then tin chloride solution was added dropwise, and the resultant mixture was stirred for two hours at room temperature. The precipitate formed was rinsed several times with deionised water to remove the impurities and then filtered using No:1 Whatman filter paper dried at 100^0C at room temperature. The resulting powder was calcined for one hour at 500 ^{0}C. Finally, the black-coloured Sn doped CuO nanocomposites were collected and stored for further characterization.

2.5. Material characterizations

X-ray diffraction pattern for the prepared nanoparticles and nanocomposites was analyzed using an X-ray diffractometer (X'Pert Pro - PAnlytic) using Cu K_α radiation of wavelength λ=0.1541 nm in the scan range 2θ=10-80°. Morphology of the nanoparticles was

analyzed using SEM (SNE- 3200M, SEC). The absorption spectra of prepared nanoparticles were recorded using a UV-VIS spectrophotometer (Thermofisher Evaluation 220). The FTIR of prepared nanoparticles were recorded using a FTIR spectrophotometer (Thermo Nicolet 380). The electrochemical capacitive behaviour has been examined using a (CH – Instrument) electrochemical work station.

3. Results and discussions

3.1. Structural studies

The phase purity and crystalline quality of the as-synthesised products were diligently inspected using X-ray diffraction. The planes are 110, 111, 200, 202, 020, 202, 113, 311, 113, 312, and 222. There was quite a good correlation between the diffraction peaks at 32.49°, 35.48°, 46.26°, 48.78°, 53.55°, 58.19°, 61.53°, 66.84°, 72.06°, and 75.39° and the typical patterns of monoclinic CuO crystalline structures (JCPDS card no. 48-1548) [14]. Similarly, the rutile phase (JCPDS No. 41-1445) exhibited the SnO_2 tetragonal structure, with peaks at 26.76°, 34.06°, 38.13°, 51.95°, 54.05°, 58.04°, 62.11°, 64.85°, 66.18°, 71.38°, and 78.82°. The planes with this geometry were (110), (101), (200), (211), (220), (002), (310), (112), (301), (202), and (321) [15].The development of the. Sn doped CuO nanocomposite is confirmed by the unambiguous visibility of two sets of planes, such as tetragonal SnO2 and cubic CuO, in Figure 1c. Cu^{2+} and Sn^{+4} are prone to undergo structural substitution in the CuO crystal lattice because of their similar effective ionic radii of 0.71 Å and 0.69 Å [33]. Sn has been assimilated into the CuO crystal structure in our case, as evidenced by the size of the crystallites and significant peak alterations [16]. Using Scherer's equation 1, the grain sizes were calculated using the full width at half-maximum (FWHM) of the peaks.

$$D = \frac{0.9\lambda}{\beta\cos\theta} \tag{1}$$

where D is the crystallite size in nm, β is the full width at half maximum (FWHM), λ is the wavelength of the X-rays (1.5406 Å), and θ is the diffraction peak angle. The estimated D value for CuO, SnO_2 and Sn doped CuO nanocomposite was found to be 6nm, 21nm, and 29nm, respectively.

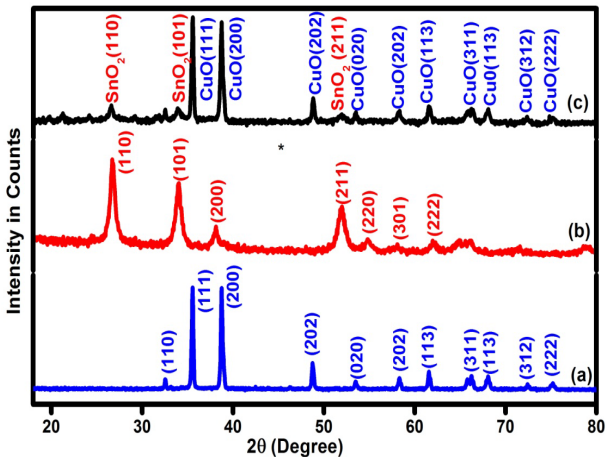

Fig. 1. XRD of (a) CuO Nps, (b) SnO_2Nps, (c) Sn doped CuO nanocomposite.

3.2. Fourier transforms infrared spectroscopy

The chemical nature has been verified using FTIR spectra. The FTIR analysis results of pure CuO, SnO nanoparticles and Sn doped CuO nanocomposite is shown in Fig. 2. In the fig 2a.narrow bands at 462 cm^{-1} and 581 cm^{-1}, intense Cu-O stretching vibrations result in the

production of exceptionally pure CuO nanoparticles [17]. The O-H bending is indicated by the peak at 1469 cm^{-1} , and the C-O stretching of phenolic and alcoholic compounds is related to the band at 1107 cm^{-1} [18, 19]. In Fig. 2b. the anti-symmetric Sn-O-Sn stretching is responsible for the band formed betweenn 450 cm^{-1} and 790 cm^{-1} [20] . The peaks at 3405 cm^{-1}, 2931 cm^{-1}, and 1623 cm^{-1}.which are brought on by the regular polymeric stretching vibration of the O-H group, indicate the presence of hydroxyl ions or maybe adsorbed water [21, 22]. Figure 2c displays the results of the Sn doped CuO nanocomposite's FTIR investigation. All identified bands are found to be pushed towards a higher wave-number side when compared to CuO nanoparticles. This shift could be due to Sn doping ions in the CuO host lattice [16].The presence of CuO nanoparticles is confirmed by the band at 526 cm^{-1} [8], whereas the C-O stretching of phenol and alcoholic compounds is the cause of the band at 1109 cm^{-1} [23].

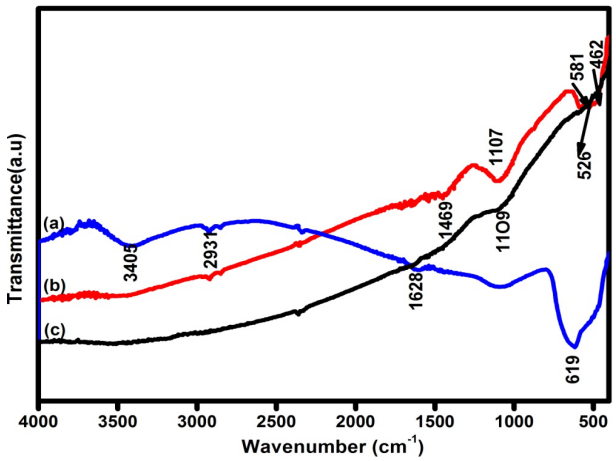

Fig. 2. FTIR of (a) CuO Nps (b) SnO_2 Nps (c) Sn doped CuO nanocomposite.

3.3. UV-visible spectrometer studies

CuO, SnO_2, and Sn-doped CuO samples' optical characteristics were examined using the UV-visible diffuse reflectance spectrum. At room temperature, the spectra were taken between 200 and 900 nm in the wavelength range. Tauc's formula (α hν) 2 = A (hν – Eg) n, where α is the absorption coefficient, hν is the photon energy, A is the constant, and n is the exponent, can be used to determine the optical band gap energy (Eg) value of the samples, depending on the kind of transition. CuO, SnO_2, and Sn-doped CuO nanocomposites are plotted on a Tauc's plot (Figs. 3a, 3b, and 3c), and band gap values are computed. It turned out that the band gaps of the biologically produced CuO and SnO_2 nanoparticles were 2.8 eV [24] and 3.9 eV [25]. It is evident that the produced CuO and SnO_2 nanoparticles show a red shift and a blue shift, respectively. Due to Sn's incorporation into the CuO lattice, it was evident that the band gap of the Sn-doped CuO nanocomposite was 1.7 eV lower than that of the pure CuO nanoparticles. Additionally, the difference in the nanoparticles' sizes could be the cause [26]. Therefore, it follows that visible light has the ability to activate copper oxide. Optoelectronic devices use these materials in many applications. Doping the photocatalyst to lower its band-gap energy improves its performance by stopping the recombination of electron-hole pairs [27].

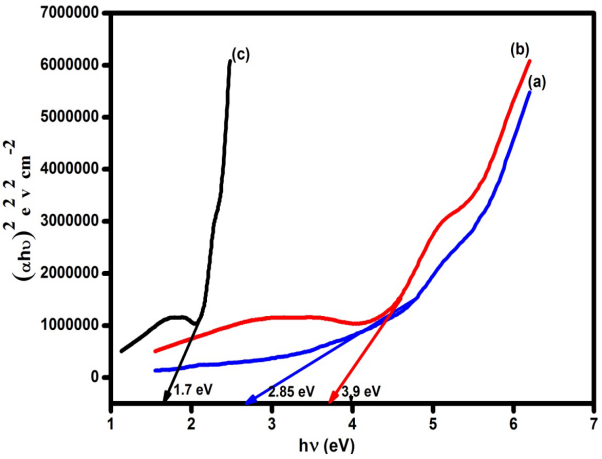

Fig. 3. Tauc plot of (a) CuO Nps (b) SnO_2Nps (c) Sn doped CuO nanocomposite.

3.4 Morphological and elemental analysis

The prepared sample's compositional analysis using the EDAX spectrum and its morphology as obtained by the FESEM are displayed in Figures 4 and 5. While pure CuO nanoparticles have leaf-like structures and minuscule particles that are agglomerated to exhibit magnetic attributes, SnO_2 nanoparticles have a rectangular rod-like morphology. CuO nanoparticles doped with Sn have a structure akin to a flaky rod. The elemental presence of generated nanoparticles is assessed using the EDAX spectrum in order to validate the presence of pure CuO and SnO_2 nanoparticles. 16.64 percent O, 74.69 percent Sn, 33.21 percent O, and 66.79% Cu are found in it. When Sn is incorporated into CuO nanoparticles, 18.23% oxygen, 8.49% tin, and 59.41% copper occur. The plant extract is probably the reason for the trace amounts of phosphorus and sulphur. The carbon-coated copper support grid exploited in the EDAX analysis is the root cause of the C peaks in the spectrum [28].

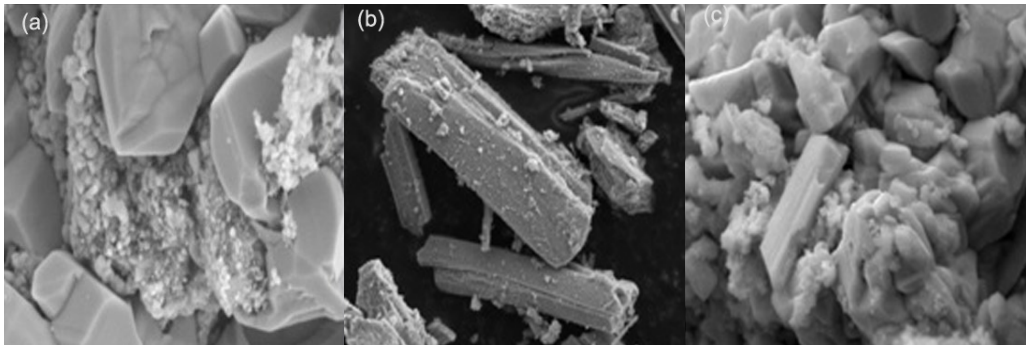

Fig. 4. FESEM of (a) CuO Nps (b) SnO_2Nps (c) Sn doped CuO nanocomposite.

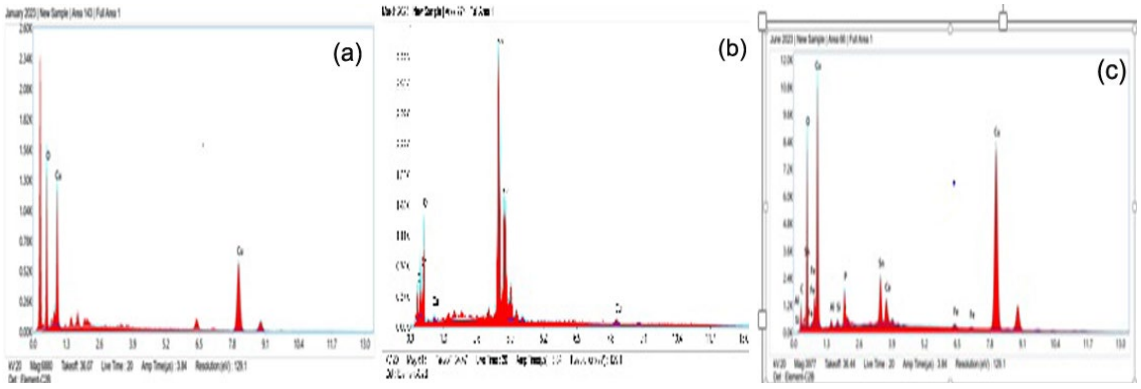

Fig. 5. EDAX of (a) CuO Nps (b) SnO_2Nps (c) Sn doped CuO nanocomposite.

3.5 Magnetic properties

Figure 6 shows the results of a measurement on pure CuO, SnO_2, and Sn-doped CuO samples using a Vibrating Sample Magnetometer (VSM)-250. The undoped CuO nanoparticles' magnetization experiments indicate a ferromagnetic order [29] at room temperature, with saturation magnetization, retentiveness, and coercive field values of MS~ 0.00329 emu/g, MR~ 0.00163 emu/g, and HC~ 0.051172, respectively. These findings are noteworthy. The presence of SnO_2 nanoparticles suggests that the sample exhibits diamagnetic characteristics [30]. Upon Sn doping, the ferromagnetic nature of CuO nanoparticles is gradually replaced by a super paramagnetic contribution, which may be arising from the presence of uncompensated Cu ions at the surface of the particles [31].

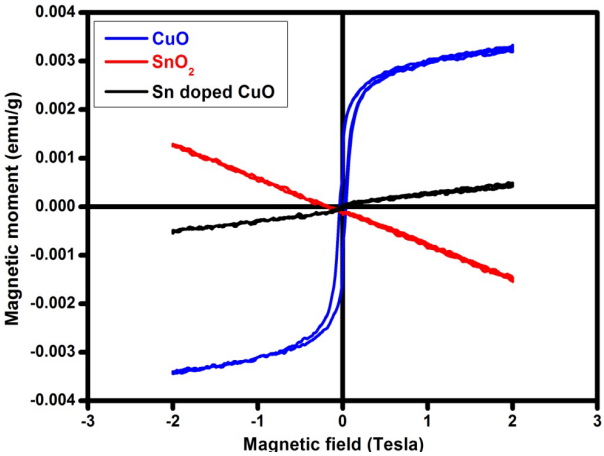

Fig. 6. VSM of (a) CuO Nps (b) SnO_2Nps (c) Sn doped CuO nanocomposite.

3.6 The electrochemical analysis

The electrochemical behaviour of CuO, SnO_2, and Sn doped CuO nanocomposites samples has been assessed by means of cyclic voltammetry. Graphite plates were employed as the counter electrode, and Ag/AgCl reference electrodes were placed in a 2 M KOH electrolyte at various rates of scanning to measure the samples using a three-electrode setup performing within the 0.1–0.6 V potential window.

Using Equation (2), the specific capacitance Csp (F/g) was computed. [22, 21]

$$\mathbf{C}sp = \int \frac{I\Delta t}{mv\Delta V} \tag{2}$$

where I is the current (A), Δt is the discharge time (s), m is the mass of active material (mg), v is the scan rate (mV/s), and ΔV is the potential window (V).

Figure 7 shows the potential range of 0.1V–0.6V for the CuO, SnO_2, and Sn/CuO nanocomposites CV curves in the 2M KOH electrolyte at various scan speeds of 10 mV/s. The region beneath the CV curve gradually expands as the scan rate rises. At a scan rate of 10 mVs^{-1}, the graph indicates that the maximum specific capacitances of CuO, SnO, and Sn doped CuO nanocomposites are approximately 175.15 Fg^{-1}, 244.60 Fg^{-1}, and ~187.64 Fg^{-1}, while the minimum specific capacitances at a scan rate of 100 mVs^{-1} are approximately 49.02 Fg^{-1}, 123.02 Fg^{-1}, and ~83.268 Fg^{-1}. When scanned at a rate of 10 mV/s, each sample in Figure 7 has a high capacitance value. It is noteworthy that in Sn-doped CuO nanocomposite, the specific capacitance value increases more than in CuO nanoparticles. The chemical and physical properties of CuO NPs can be altered by the addition of the dopant Sn. In both cases, the anodic and cathodic peak currents gradually increase as scan speeds increases. A graph of peak current vs scan rate is created, as seen in Figure 8, to validate the electrode procedure. For every metal oxide, a linear line can be seen, suggesting that the mechanism for charge storage was a diffusion-controlled

redox process. [32]. Electrochemical redox parameter from cyclic voltammetric studies was given by Table 1.

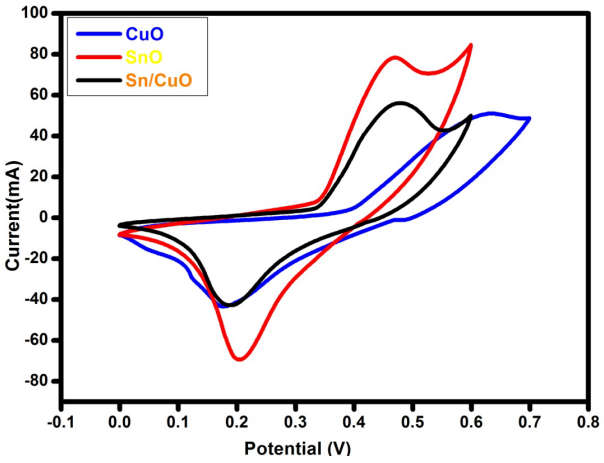

Fig. 7. CV Studies of CuO Nps, SnO_2Nps & Sn doped CuO nanocomposite.

For the CuO, SnO_2, and Sn doped CuO nanocomposites, the oxidation peak currents were 49.3882 µA, 80.0481 µA, and 58.0828 µA, whereas the reduction peaks were -49.2726 µA, -75.2649 µA, and -48.6319, according to the scan rate at 10 mV/s. The Sn/CuO nanocomposite appears to have greater current responsiveness when compared to CuO nanoparticles. Sn doped CuO nanocomposite had superior electrocatalytic efficacy than CuO nanoparticles because oxidation was more beneficial in this case. Reversible electrochemical processes are shown by almost equal ratios (Ipa/Ipc) between peak currents at the anode and cathode responses for each sample [33].

Table. 1. Electrochemical redox parameters from cyclic voltammetric studies at the scan rate of 10mV/s.

Name	i_{pa} µA	i_{pc} µA	E_{pa}	E_{pc}	E_{pa}-E_{pc}	I_{pa}/i_{pc}
CuO	49.3882	-49.2726	0.6891	0.1792	0.440	1
SnO_2	80.0481	-75.2649	0.4657	0.20479	0.260	1
Sn/CuO	58.0828	-48.6319	0.4728	0.18368	0.289	1.19

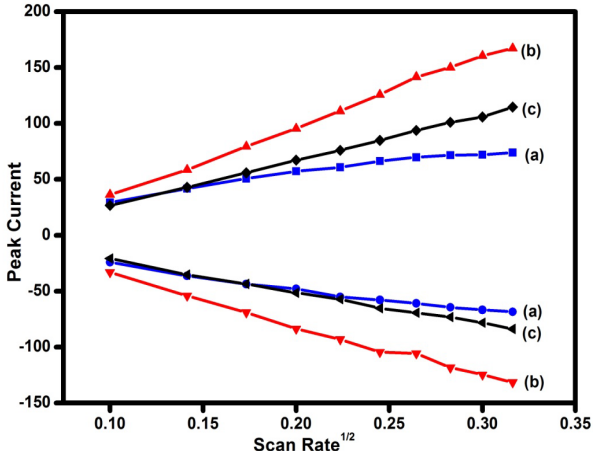

Fig. 8. Plot of peak current versus square root of scan rate ((a) CuO Nps (b) SnO_2Nps (c) Sn doped CuO nanocomposite).

3.7. Antibacterial studies

Gram-positive and Gram-negative microorganisms were tested to determine the antibacterial activity of CuO NPs (KC), SnO_2NPs (SN) and Sn doped CuO (KSN) nanocomposites made from *Centratherum punctuatum* leaf extract. The disk diffusion method carries out antibacterial action. After being injected into peptone water, the test bacteria were cultured at 35 ^oC for three to four hours. Sterile Petri dishes were filled with prepared Muller-Hinton agar plates. On the surface of the Mueller-Hinton agar plates, 0.1 ml of bacterial culture was injected and distributed using an L-rod. Five minutes were given to the infected plates to dry. Using a sterile procedure, the disk containing samples at a concentration of 1000 µg/ml was deposited on the surface of Petri plates that had been inoculated. For 18 to 24 hours, the plate was incubated at 37 ^oC. The inhibitory zone on the plate was found, and its measurement in millimeters was made. Because their mechanism depends not only on the metal oxide nanoparticles but also on the tested bacterial species [34], the concentration and size of the nanoparticles are critical to their antibacterial efficacy [35]. In fig. 9 Gram-positive bacteria like *Staphylococcus aureus* and *Bacillus stereus*, as well as gram-negative bacteria like *Escherichia coli* and *Pseudomonas aeruginosa*, were the subjects of antibacterial investigations for CuO NPs, SnO_2 NPs, and Sn doped CuO nanocomposites. As Table 2 illustrates, it was found that all samples were more successful in combating gram-negative bacteria than gram-positive bacteria [36]. Furthermore, the antibacterial activity of Sn doped CuO nanocomposites is similar to pure CuO nanoparticles.

Table 2. Antibacterial activity data for the CuO, SnO_2 and Sn doped CuO.

Bacteria	Inhibition zone in mm		
	CuO (KC)	SnO_2 (SN)	Sn dopedCuO (KSN)
E.coli	12	Nil	13
Staphylococcus aureus	15	Nil	13
Bacillus cereus	14	Nil	11
Pseudomonas aeruginosa	12	Nil	12

Fig. 9. Antibacterial studies of CuO Nps, SnO_2 Nps & Sn doped CuO nanocomposite.

4. Conclusion

This work showed how to synthesize CuO-NPs, SnO_2 NPs, and Sn doped CuO nanocomposites in an environmentally friendly, straightforward, and effective manner utilizing *Centraturam punctuatum* leaf extract. XRD confirms that when Sn is introduced to copper oxide nanoparticles, the size of the particles rises. Sn doped CuO nanocomposites have a reduced optical band gap of 1.7 eV in the UV-visible spectrum. The presence of metal oxide nanoparticles and a shifted wavenumber to the upper area in Sn doped CuO nanocomposites are confirmed by FTIR. According to FESEM photos, SnO2 nanoparticles have a rectangular rod-like morphology, CuO nanoparticles doped with Sn have a shape analogous to a flaky rod, and CuO nanoparticles form leaf-like structures. EDAX spectroscopy is used to establish the elemental composition of nanomaterials. Studies using cyclic voltammetry verify the pseudocapacitance nature of the Sn doped copper oxide nanocomposite by demonstrating a high specific capacitance.

Because of its great electrochemical stability, it can therefore be employed as a potential electrode for supercapacitor applications. Ferromagnetic behavior in CuO nanoparticles was reported in VSM investigations, and in Sn doped CuO nanocomposite, this behaviour transforms into superparamagnetic nature. The magnetic measurements unequivocally show that super paramagnetism exists in nanocomposites, which may be caused by uncompensated Cu ions present on the particle surface. In conclusion, the green synthesis of nanomaterial particles that resulted showed significant antibacterial activity, suggesting potential applications in food packaging, medicine, and sufficient defense against pathogen

Acknowledgements

S. Subha (Reg,No: 19122232132023) is thankful to authorities of V.O.Chidambaram College, Thoothukudi and Manonmaniam Sundaranar University, Abishekapatti, Tirunelveli, Tamilnadu, India for providing necessary research facilities.

References

[1] L. Yanwu, O. Yip, L. Fangxin, Rare Metals **25**(6), 493 (2006); https://doi.org/10.1016/S1001-0521(07)60132-6.
[2] S. Mohebbi, S. Molaei, A. R. J. Azar, Journal of Applied Chemistry **8**(27), 27 (2013).
[3] M. Ramzan, R. M. Obodo, S. Mukhtar, S. Z. Ilyas, F. Aziz, N. Thovhogi, Materials Today Proceedings 35(2), 576 (2021); https://doi.org/10.1016/j.matpr.2020.05.472.
[4] P. Vomacka, V. Stengl, J. Henych, M. Kormunda, Journal of Colloid and Interface Science **481,** 28 (2016); https://doi.org/10.1016/j.jcis.2016.07.026.
[5] S. S. Gunasekaran, A. Gopalakrishnan, R. Subashchandrabose, S. Badhulika, Journal of Energy Storage 37, 102412 (2021). http://doi.org/10.1016/j.est.2021.102412.
[6] S. Gnanam, V. Rajendran, Journal of Sol-Gel Science and Technology **56**, 128 (2010); https://doi.org/10.1007/s10971-010-2285-7.
[7] M. Hafeez, R. Shaheen, B. Akram, M. N. Ahmed, S. Haq, S. U. Din, M. Zeb, M. A. Khan. South African Journal of Chemistry **75**(1), 168 (2021); https://doi.org/10.17159/0379-4350/2021/v75a21
[8] K. Sofiya Dayana, R. Jothi Mani, S. C. Vella Durai, Digest Journal of Nanomaterials and Biostructures **16**(3), 1119 (2021); https://doi.org/10.15251/DJNB.2021.163.1119
[9] O. H. Abdullah, A. M. Mohammed, Digest Journal of Nanomaterials and Biostructures **15**(3), 943 (2020); https://doi.org/10.15251/DJNB.2020.153.943
[10] A. A. Salih, W. K. Abad, S. A. Fadaam, B. H. Hussein, , Digest Journal of Nanomaterials and Biostructures **18**(4), 1225 (2023); https://doi.org/10.15251/DJNB2023.184.1225.
[11] N. K. Pawar, N. Arumugam, Asian Journal of Pharmaceutical and Clinical Research **4**(3), 71 (2011).

[12] B.Chitra, P. Brindha, International Journal of Pharmacy and Pharmaceutical Sciences **6** (1), 19 (2014).
[13] S. G. Firisa, G. G. Muleta, A. A. Yimer,, ACS Omega **7**(49), 44720 (2022); https://doi.org/10.1021/acsomega.2c04042.
[14] R. Chowdhury, A. Khan, M. H. Rashid, RSC Advances 10, 14374 (2020); https://doi.org/10.1039/D0RA01479F.
[15] P. A. Luque, O. Nava, C. A. Soto-Roblesa, M. J. Chinchillas-Chinchillasa, H. E. Garrafa-Galvezb, Y. A. Baez-Lopeza, K. P. Valdez-Núñezc, A. R. Vilchis-Nestord, A. Castro-Beltránb, Optik **206,** 164299 (2020); https://doi.org/10.1016/j.ijleo.2020.164299.
[16] R. D. Shannon, Acta Crystallographica Sect. A **32**, 751 (1976); http://dx.doi.org/10.1107/S0567739476001551.
[17] K. Sofiya Dayana, R. Jothimani, S. C. Vella Durai, Journal of Nano and Electronic Physics, **13(**1), 01014 (2021); https://doi.org/10.21272/jnep.13(1).01014.
[18] V. U. Siddiqui, A. Ansari, R. Chauhan, W. A. Siddiqi, Materials Today Proceedings **36**(3), 751 (2021); https://doi.org/10.1016/j.matpr.2020.05.504.
[19] A. Varughese, R. Kaur, P. Singh, IOP Conference Series: Materials Science and Engineering **961,** 012011 (2020); https://doi.org/10.1088/1757-899X/961/1/012011.
[20] P. A. Luquea, M. J. Chinchillas-Chinchillasb, O. Navaa, E. Lugo-Medinac, M. E. Martínez-Rosasa, A. Carrillo-Castillod, A. R. Vilchis-Nestore, L. E. Madrigal-Mu˜noza, H. E. Garrafa-G´alveza, Optik **229,** 166259 (2021); https://doi.org/10.1016/j.ijleo.2021.166259.
[21] J. Yang, K. Yang, L. Qiu, Environmental Toxicology and Pharmacology **44**, 48 (2017); https://doi.org/10.1016/j.etap.2017.06.013
[22] T. Petrov, I. M. Deneva, O. Chauvet, R. Nikolov, I. Denev, Journal of the University of Chemical Technology and Metallurgy **47(**2), 197 (2012).
[23] G, Paramasivam, P. S. Karnan, S. Subbiah, S. N. Somasundaram, S. M. Paulraj, International Journal of Research in Advent Technology **7(**5S), (2019).
[24] A. T. Babu, R. Antony, Journal of environmental chemical engineering **7(**1), 102840 (2019); https://doi.org/10.1016/j.jece.2018.102840.
[25] E. Gomathi, M. Jayapriya, M. Arulmozhi, Inorganic Chemistry Communications **130**, 108670 (2021); https://doi.org/10.1016/j.inoche.2021.108670.
[26] V. Kumar, S. Senb, K. P. Muthe, N. K. Gaur, S. K. Gupta, J. V. Yakhmi, Sensors and Actuators B: Chemical **138**, 587 (2009); https://doi.org/10.1016/j.snb.2009.02.053.
[27] A. T. Babu, R. Antony, Journal of Environmental Chemical Engineering, **7(**1), 102840 (2019); https://doi.org/10.1016/j.jece.2018.102840.
[28] S. G. Firisa, G. G. Muleta, A. A. Yimer, ACS Omega **7**(49), 44720 (2022); https://doi.org/10.1021/acsomega.2c04042.
[29] K. Chakrabarti, B. Sarkar, V. D. Ashok, K. Das, S. S. Chaudhuri, S. K. De, Nanotechnology **24**, 505711 (2013); https://doi.org/10.1088/0957-4484/24/50/505711.
[30] A. Sundaresan, R. Bhargavi, N. Rangarajan, U. Siddesh, C. N. R. Rao, Physical Review B **74**, 161306R (2006); https://doi.org/10.1103/PhysRevB.74.161306.
[31] G. Narsinga Rao, Y. D. Yao, J. W. Chen, IEEE Transactions on Magnetics **41(**10), 3409 (2005); https://doi.org/10.1109/TMAG.2005.855214.
[32] M. W. Alam, M. Aamir, M. Farhan, M. Albuhulayqah, M. M. Ahmad, C. R. Ravikumar, V. G. Dileep Kumar, H. C. Ananda Murthy, Crystals **11(12)**, 1467 (2021); https://doi.org/10.3390/cryst11121467.
[33] E. C. Okpara, O. E. Fayemi, Materials Research Express 6(10), 105056 (2019); https://doi.org/10.1088/2053-1591/ab3abb.
[34] A. Hassen, N. Saidi, M. Cherif, A. Boudabous, Bioresource Technology **65**(1–2), 73(1998); https://doi.org/10.1016/S0960-8524(98)00011-X.
[35] Z. Sabouri, A. Akbari, H. A. Hosseini, A. Hashemzadeh, M. Darroudi, Journal of Cluster Science **30**, 1425 (2019); https://doi.org/10.1007/s10876-019-01584-x.
[36] R. Radhakrishnan, F. L. A. Khan, A. Muthu, A. Manokaran, J. S. Savarenathan, K. Kasinathan, Letters in Applied Nano Bio Science, **10**(4), 2706 (2021); https://doi.org/10.33263/LIANBS104.27062714.